HHS Public Access

Author manuscript

J Biomol NMR. Author manuscript; available in PMC 2019 October 01.

Published in final edited form as:

J Biomol NMR. 2018 October ; 72(1-2): 39–54. doi:10.1007/s10858-018-0205-2.

Correlated Motions of C'—N and C_α—C_β pairs in Protonated and Per-deuterated GB3.

Liliya Vugmeyster[a,*], **Aaron Griffin**[a], **Dmitry Ostrovsky**[b], **Shibani Bhattacharya**[c], **Parker J. Nichols**[d], **C. James McKnight**[e], and **Beat Vögeli**[d]

[a]Department of Chemistry, University of Colorado at Denver, Denver, CO 80204

[b]Department of Mathematics, University of Colorado at Denver, Denver, CO 80204

[c]New York Structural Biology Center, New York, NY 10027

[d]Department of Biochemistry and Molecular Genetics, University of Colorado, School of Medicine, Anschutz Medical Campus, Aurora, CO, 80045

[e]Departmentof Physiology and Biophysics, Boston University School of Medicine, Boston, MA, 02118

Abstract

We investigated correlated μs-ms time scale motions of neighboring $^{13}C'$—^{15}N and $^{13}C_\alpha$—$^{13}C_\beta$ nuclei in both protonated and perdeuterated samples of GB3. The techniques employed, NMR relaxation due to cross-correlated chemical shift modulations, specifically target concerted changes in the isotropic chemical shifts of the two nuclei associated with spatial fluctuations. Field-dependence of the relaxation rates permits identification of the parameters defining the chemical exchange rate constant under the assumption of a two-site exchange. The time scale of motions falls into the intermediate to fast regime (with respect to the chemical shift time scale, 100 to 400 s^{-1} range) for the $^{13}C'$—^{15}N pairs and into the slow to intermediate regime for the ^{13}C—α$^{13}C_\beta$pairs (about 150 s^{-1}) . Comparison of the results obtained for protonated and deuterated GB3 suggests that deuteration has a tendency to reduce these slow scale correlated motions, especially for the $^{13}C_\alpha$—$^{13}C_\beta$ pairs.

Keywords

correlated motions; cross-correlation NMR relaxation; GB3; protein dynamics; deuteration

Introduction

Cross-correlated chemical shift modulation (CSM/CSM) is an analog of chemical exchange (the movement of nuclei between environments) for multi-nuclei coherences and reflects concerted fluctuations in the chemical shift of pairs of nuclei due to local motions. If the chemical shifts of both nuclei move in the same direction they are correlated, and if they move in opposite directions they are termed anti-correlated. The CSM/CSM technique has

*corresponding author: LILIYA.VUGMEYSTER@UCDENVER.EDU; 1201 Larimer Street, Denver Colorado, 80204.

been applied to several proteins including ubiquitin, BPTI, calmodulin C-terminal domain, dematin headpiece, chicken villin headpiece subdomain, and major urinary protein. (Brutscher et al. 1998; Fruh et al. 2001; Lundstrom and Akke 2004; Lundstrom et al. 2005; Majumdar and Ghose 2004; Pellecchia et al. 1999; Perazzolo et al. 2005; Vugmeyster 2009; Vugmeyster and McKnight 2009; Vugmeyster et al. 2004; Wang and Palmer 2002; Wist et al. 2004; Wist et al. 2005) Different pairs of nuclei were investigated, including neighboring ^{1}H—^{15}N, $^{13}C'$—^{15}N, $^{13}C_{\alpha}$—$^{13}C_{\beta}$, $^{13}C'$—$^{13}C_{\alpha}$, as well as $^{13}C_{\alpha}/^{13}C_{\alpha}$ in adjacent residues.

In this work we investigated concerted motions of $^{13}C'$—^{15}N backbone pairs and $^{13}C_{\alpha}$—$^{13}C_{\beta}$ pairs in protonated and in per-deuterated samples of the third IgG-binding domain of Protein G (GB3), a model 56 residue protein (Derrick and Wigley 1994). The secondary structure of GB3 is comprised of four β-sheets (residues 2–8, 13–19, 42–46, 51–55) and an α-helix (residues 23–37). The pulse sequences for the crosscorrelated experiments have been previously developed. (Brutscher et al. 1998; Fruh et al. 2001; Pellecchia et al. 1999; Wist et al. 2004; Wist et al. 2005)

The concerted changes in the isotropic chemical shift can be caused by a variety of phenomena. For the $^{13}C'$— ^{15}N backbone case, examples include variations of φ and ψ dihedral angles of the backbone, slow collective motions of protein domains, dynamic intramolecular interactions, transient hydrogen bonds, and transient interactions between complexes or fluctuating interactions with metal ions. (Arnold and Oldfield 2000; Frueh 2002; Kateb et al. 2006) For the $^{13}C_{\alpha}$—$^{13}C_{\beta}$ case, examples of such processes are rotameric jumps, slow collective motions of the core, or local motions of neighboring bulky groups.

There are a number of considerations which make data collection and analysis more difficult for the$^{13}C_{\alpha}$— $^{13}C_{\beta}$ experiment compared with the $^{13}C'$— ^{15}N case. First, the magnetization is transferred from the amide proton all the way along the backbone to the C_{β} atom, thus considerably decreasing the sensitivity of the experiment. Second, the resulting coherences have a J-coupling modulation during the relaxation period for side-chains with aliphatic Cγ carbon(s). While it complicates the analysis, it allows for the extractions of $^{1}J(C_{\beta}C_{\alpha})$ and$^{2}J(C_{\alpha}C_{\gamma})$ scalar coupling constants. Third, as we will see, quantitative extraction of the CSM/CSM terms requires a precise estimate of $^{13}C_{\alpha}$ and $^{13}C_{\beta}$ chemical shift anisotropy tensors and their relative orientations, which are difficult to quantify. ^{15}N and $^{13}C'$ tensor parameters have been more extensively studied and Loth et al. (Loth et al. 2005) have developed a set of rules relating tensor components to isotropic chemical shift values. For GB3 ^{15}N tensors have been extensively characterized by Fushman and coworkers.(Hall and Fushman 2006)

Field dependence of the CSM/CSM rates imposes constraints on the time scale of motions. Single quantum (SQ) R_{ex} field dependence was analyzed in detail by Millet et al. (Millet et al. 2000). Wang and Palmer extended the technique to MQ coherences using ^{1}H—^{15}N spin pairs (Wang and Palmer 2002). By performing the measurements at two static fields and building upon the theoretical equations in (Wang and Palmer 2002), we derive constraints for the upper limits of the chemical exchange rate constants of the $^{13}C'$— ^{15}N and $^{13}C_{\alpha}$—$^{13}C_{\beta}$ pairs in GB3. For most CSM/CSM data reported in the literature, the conformational exchange was either demonstrated to fall into the fast limit with respect to the chemical shift

time scale or this limit was assumed to be valid. A notable exception is the case of BPTI, in which the exchange rate constant for $^{1}H–^{15}N$ MQ coherence was found to fall into slow to intermediate exchange regime (Wang and Palmer 2002). We show that in our case the field dependence suggests clear deviations from the fast exchange regime.

Further, we perform measurements in both protonated and perdeuterated GB3 proteins. In many biophysical studies which employ deuteration it is implicitly assumed that deuteration of nonexchangeable protons does not alter dynamics or intermolecular interactions. Our data suggest that there could be differences in the dynamics of slow concerted fluctuations between protonated and deuterated proteins, especially for pairs of nuclei directly attached to the deuterons such as C_α—C_β pairs.

Materials and Methods

Sample Conditions

Protonated sample is homogenously $^{13}C/^{15}N$-labeled protein expressed in 100% H_2O as described (Vögeli et al. 2008). The protonated sample concentration was around 4 mM. The perdeuterated sample corresponds to homogenously $^{13}C/^{15}N/^{2}H$-labeled GB3 expressed using the same method as for the protonated sample except that it was carried out in 99.8% D_2O instead of H_2O and using $^{13}C/^{2}H$ labeled glucose. The sample concentration was around 2.4 mM. The buffer conditions are the following: 50 mM sodium phosphate buffer, 50 mM NaCl, and 0.05% w/v NaN_3, at pH 7.0. The deuteration pattern of the targeted nuclei is depicted in Figure 1. All exchangeable sites, and the backbone amide hydrogens in particular, are protonated as the purification is performed in unlabeled aqueous buffers. This allows for complete exchange of backbone and side chain amide hydrogens.

Analytical Reversed-Phase HPLC data collection

Analytical reversed-phase (RP) high pressure liquid chromatography (HPLC) data collection has been conducted on an Agilent Technologies 1100 HPLC system at 25 °C with a C8 column (Zorbax 2.1 × 150 mm) and a 0.25% linear AB gradient, where eluent A was water with 0.05% trifluoroacetic acid (TFA) and eluent B was acetonitrile with 0.05% TFA. To determine the relative protein sample concentrations the absorbance at 280 nm of the peak areas of the mixture were measured. Injected amounts corresponded to about 0.43 μg of the protonated protein, and 0.54 μg of the deuterated protein. The order of the retention times was confirmed by injection of individual protonated and deuterated samples.

NMR data acquisition and processing

NMR measurements were performed on Bruker 500 MHz and 900 MHz spectrometers equipped with TCI/TXI cryoprobes (Boston University School of Medicine, Boston, MA and New York Structural Biology Center, New York, NY). All measurements were performed at 25 °C. The temperatures at the two fields were matched using proton chemical shifts. $^{13}C'$—N CSM/CSM measurements were carried out using the pulse sequence described in (Wist et al. 2004; Wist et al. 2005) with a single echo period and 8 relaxation delays (1, 3, 6, 14, 20, 32, 40, and 60 ms). The $^{13}C_\alpha$— $^{13}C_\beta$ CSM/CSM experiment employed the pulse sequence described in (Fruh et al. 2001). For the deuterated sample,

proton decoupling was replaced by deuterium decoupling for time periods in which $^{13}C—^{2}D$ couplings needed to be suppressed (Vugmeyster et al. 2004). 11 relaxation delays (2, 6, 8, 10, 14, 18, 22, 28, 34, 40, and 50 ms) were used. 2D spectra were acquired with 1024 × 80 complex points (C′N) and 1024 × 64 points (CαCβ) and 1.8 s and 7 s recycle delays for the protonated and deuterated samples, respectively. The increased recycle delay for the deuterated sample was used to guarantee near-complete return to equilibrium magnetization (Lakomek et al. 2012). For the protonated sample, duplicate data sets were collected, and the results represent the average of the two data sets. C' chemical shifts were obtained from the 3D HNCO experiment (Kay et al. 1990).

The data were processed with the NmrPipe/NmrDraw/NlinLS package (Delaglio et al. 1995). Each dimension was apodized by a 90^{o} phase-shifted sine-bell window function and zero-filled once. For the C'N experiment, ΔR rates (Eq. 1 in *Theory* section) were obtained by fitting the ratios of intensities from double quantum (DQ) and zero quantum (ZQ) spectra to a two-parameter exponential decay function. For the $C_\alpha C_\beta$ experiment, individual R_{DQ} and R_{ZQ} rates were obtained first, then combined to calculate ΔR. Residues 25, 27, 42 and 48, and 35 ($C_\alpha C_\beta$ in deuterated GB3 only), were excluded due to overlap in peak positions. Additionally, in the deuterated sample residue 54 was excluded from the $C_\alpha C_\beta$ data due to low peak intensity. For the determination of the $C_\alpha C_\beta$ rates, residues without a C_γ carbon were fitted with the two-parameter exponential decay function. For residues containing one or two aliphathic C_γ carbons, the exponential decay function was multiplied by $(\cos\pi J_{eff}\tau)^n$, in which n is the number of the C_γ carbons, τ is the variable relaxation time, and J_{eff} is the effective scalar coupling constant specified in the theoretical section. All fits and error analysis were done in Matlab (The Mathworks Inc.) using the Levenberg–Marquardt algorithm.

Determination of tumbling times

The molecular tumbling times, τ_c, were determined from R_1 and R_1 ^{15}N relaxation experiments (Cavanagh et al. 2006) at the same temperature as the multiple quantum measurements and at the two field strengths of 500 and 900 MHz. Additional ^{15}N R_2 relaxation as well as transverse relaxation-optimized spectroscopy(Lee et al. 2006) data were collected and confirmed the $R_{1\rho}$-based values. The τ_c values are 3.6 and 2.7 ns for the protonated and perdeuterated proteins, respectively, under the assumption of isotropic tumbling (see Fushman and Hall for the discussion of the limits of this approximation (Hall and Fushman 2003)).

Results and Discussion

Theoretical background for determination of CSM/CSM cross-correlated rates

In the multiple-quantum CSM/CSM experiments used in this work, the differential auto-relaxation rates, ΔR, of the double-quantum (DQ) and zero-quantum (ZQ) coherences involving two nuclei are measured:

$$\Delta R = \frac{1}{2}\left(R_{DQ} - R_{ZQ}\right) \quad (1)$$

In the case of $^{13}C'-^{15}N$ these coherences are proportional to the heteronuclear spin operators $1/2(C'_+N_+ + C'_-N_-)$ and $1/2(C'_+N_- + C'_-N_+)$, respectively. In the case of $^{13}C_\alpha—^{13}C_\beta$, the detected operators take the form of $1/2\left(4C_\alpha^+C_\beta^+N_zC'_z - 4C_\alpha^-C_\beta^-N_zC'_z\right)$ and $1/2\left(4C_\alpha^+C_\beta^-N_zC'_z - 4C_\alpha^-C_\beta^+N_zC'_z\right)$ coherences, which have relaxation properties similar to the DQ $\left(1/2\left(C_\alpha^+C_\beta^+ - C_\alpha^-C_\beta^-\right)\right)$ and ZQ $\left(1/2\left(C_\alpha^+C_\beta^- - C_\alpha^-C_\beta^+\right)\right)$ coherences. The J-coupling to aliphatic C_γ carbons is not averaged and causes a cosine modulation of the decaying coherences.

Several auto- and cross-correlated relaxation mechanisms contribute to the relaxation rates R_{DQ} and R_{ZQ}. However, the difference in the rates depends only on cross-correlated mechanisms:

$$\Delta R = R_{CSA/CSA} + R_{DD/DD} + R_{CSM/CSM} \quad (2)$$

where $R_{DD/DD}$ represents the contributions of cross-correlated dipole-dipole mechanisms involving one passive spin and $R_{CSA/CSA}$ is the contribution of the cross-correlated mechanism due to the chemical shift anisotropies. The third term, $R_{CSM/CSM}$, which is of main interest in this work, is due to correlated isotropic chemical shift modulations of the two nuclei. The "unwanted" $R_{DD/DD}$ and $R_{CSA/CSA}$ terms have to be calculated and subtracted from the measured ΔR rate to obtain the $R_{CSM/CSM}$ term.

I. Cross-correlated chemical shift modulation contribution, $R_{CSM/CSM}$—For two nuclei A and B, the chemical shift modulation Hamiltonian is given by

$$H = \delta\omega_A(t)A_z + \delta\omega_B(t)B_z \quad (3)$$

in which $\delta\omega_{A,B}(t)$ are time-dependent deviations from the isotropic chemical shifts. The relaxation contribution to ΔR due to cross-correlated chemical shift modulation is calculated using Redfield theory for the observable DQ and ZQ terms (Frueh 2002):

$$R_{CSM/CSM} = \frac{1}{2}(J^{A,B}_{CSM/CSM}(0) + J^{B,A}_{CSM/CSM}(0)) \quad (4)$$

The spectral density expresses the extent of correlation between the fluctuations of the two chemical shifts:

$$J^{A,B}_{CSM/CSM}(0) = \int_{-\infty}^{\infty}\left\langle\delta\omega_A(t)\delta\omega_B(0)\right\rangle dt \quad (5)$$

in which <…> denote ensemble average.

II. The field dependence of the $R_{CSM/CSM}$ term permits the estimation of k_{ex}. —Wang & Palmer (Wang and Palmer 2002) have shown that the $R_{CSM/CSM}$ contribution is given by Eq. 6 under the following assumptions: a) two-site exchange; b) the population of one of the sites is much smaller than the other one,$p_1 \gg p_2$; c) the k_{ex} exchange rate constant is comparable to the spin echo delay; and d) the intrinsic transverse relaxation rate is the same in both sites. This last assumption can be violated if there are differences in CSA/CSA interactions and dipolar interactions to remote spins between the two exchanging sites.

$$R_{CSM/CSM} = \frac{2p_1p_2\Delta\omega_A\Delta\omega_B k_{ex}^3}{\left(k_{ex}^2+\Delta\omega_A^2+\Delta\omega_B^2\right)^2-4\Delta\omega_A^2\Delta\omega_B^2} \quad (6)$$
$$= p_1p_2k_{ex}\frac{2\Delta\omega_A\Delta\omega_B k_{ex}^2}{\left(k_{ex}^2+\Delta\omega_A^2+\Delta\omega_B^2\right)^2-4\Delta\omega_A^2\Delta\omega_B^2}$$

In this equation, $\Delta\omega_A$and $\Delta\omega_B$ are the chemical shift differences between the two exchanging sites for nuclei A and B. Note that for the case of identical signs of γ_A and γ_B, positive $R_{\mathrm{CSM/CSM}}$ rates indicate that the chemical shift changes upon fluctuations are correlated, meaning that fluctuations of the two nuclei cause the chemical shifts to change in the same direction, while negative rates indicate anti-correlated changes of the chemical shifts. When the signs of γ_A and γ_B are opposite, positive rates indicate anticorrelated changes in the chemical shifts upon fluctuations. In the same limit, the expression for the chemical exchange of the single quantum coherence for one of the nuclei, R_{ex}, is given by:

$$R_{ex} = \frac{k_{ex}\Delta\omega_A^2 p_1p_2}{k_{ex}^2+\Delta\omega_A^2} \quad (7)$$

In the fast exchange limit, $\frac{k_{ex}}{\sqrt{\Delta\omega_A^2+\Delta\omega_B^2}} \gg 1$, $R_{CSM/CSM}$ becomes:

$$R_{CSM/CSM} = \frac{2p_1p_2\Delta\omega_A\Delta\omega_B}{k_{ex}}. \quad (8)$$

Field dependence of the $R_{CSM/CSM}$ term, given for example by the ratio of $R_{CSM/CSM}$ at two values of the static magnetic field strength, provides constraints on the time scale of the exchange process compared with the chemical shifts time scale, in analogy to what has been derived for the SQ coherence (Millet et al. 2000). The use of assumption b) above permits the elimination of the factor when considering the fielddependence. The relative values of $\Delta\omega_A$ and $\Delta\omega_B$ greatly affect the interpretation of the field dependence of the results. When $\Delta\omega_A$ and $\Delta\omega_B$ are of comparable magnitude, similarity to the SQ case is obtained (Millet et al. 2000): Quadratic field dependence implies fast exchange (as implicated by equation 8), no field dependence indicates slow exchange, and linear field dependence indicates

intermediate exchange. When the magnitudes of $\Delta\omega_A$ and $\Delta\omega_B$ are very different from each other, the situation becomes more complex. For example, in the slow exchange regime it is possible to obtain field dependence with the factor of proportionality less than 1.

The ratio of $R_{CSM/CSM}$ at two fields may be parameterized with the dimensionless quantities $\tilde{k}_{ex} = \frac{k_{ex}}{\sqrt{\Delta\omega_A^2 + \Delta\omega_B^2}}$ and $r = \frac{2\Delta\omega_A\Delta\omega_B}{\Delta\omega_A^2 + \Delta\omega_B^2}$. $\tilde{k}_{ex}$ is itself field dependent and provides information on the rate of exchange on the chemical shift scale. r depends only on the relative values of $\Delta\omega_A$ and $\Delta\omega_B$. r is defined in such a way that r^2 value can range between 0 and 1: $r^2 = 1$ for $\Delta\omega_A = \Delta\omega_B$ and $r^2 = 0$ when the chemical shift changes are very different.

Figure 2 demonstrates the field dependence of the $R_{CSM/CSM}$ term according to Eq. 6 as a function of $\tilde{k}_{ex}$. The example is shown for the two field strengths of 900 and 500 MHz, which are used in the experiment. Chemical shifts are taken at 500 MHz. The results are shown as a function of the parameter r^2. The sigmoidal shape of the curves in Figure 2 reflects the crossover behavior of $R_{\mathrm{CMC/CMS}}$ from the slow to fast exchange regimes.

Eq. 6 in combination with the field dependence of the $R_{CSM/CSM}$ permits us to estimate the lower and upper limits on the values of k_{ex}. While the ratio of $R_{CSM/CSM}$ at two fields provides limits on possible values of $\frac{k_{ex}}{\sqrt{\Delta\omega_A^2 + \Delta\omega_B^2}}$, in order to obtain the typical values of k_{ex} additional assumptions are needed.

To obtain the maximum possible value of k_{ex} one needs a good estimate of the upper limits of $\Delta\omega_A$ and $\Delta\omega_B$. The typical maximum expected values of $\Delta\omega$ resulting from conformational exchange, based on the BMRB statistics as well as discussions in (Iwadate et al. 1999; Le and Oldfield 1994) are the following: ^{13}C' - 10 ppm, ^{15}N - 15 ppm, C_α and C_β around 6.5 ppm (5 ppm due to backbone, 1 ppm due to H-bonding, 0.5 ppm due to side chain fluctuation). We will use these values when interpreting experimental data.

We will now explain the determination of the lower limit of k_{ex} when $R_{CSM/CSM}$ terms at two fields are known experimentally.

Eq. 6 can be written as

$$R_{CSM/CSM} = p_1 p_2 \, k_{ex} F \quad (6b)$$

where $F = \frac{2\Delta\omega_A\Delta\omega_B k_{ex}^2}{\left(k_{ex}^2 + \Delta\omega_A^2 + \Delta\omega_B^2\right)^2 - 4\Delta\omega_A^2\Delta\omega_B^2}$.

F can be rewritten as a function of the two variables r and $\tilde{k}_{ex}$:

$$F = \frac{r\tilde{k}_{ex}^2}{(1+\tilde{k}_{ex}^2)^2 - r^2}$$

The ratio of $R_{CSM/CSM}$ values at two fields is equal to the ratio of the corresponding F factors. Also, as was shown in Figure 2, the ratio of $R_{CSM/CSM}$ determines the $\tilde{k}_{ex}$ value, which, by itself, cannot be used to extract the k_{ex} value or its lower limit because of the uncertainties in the chemical shift differences. However, when $\tilde{k}_{ex}$ is known and a reasonable assumption can be made about the value of , one can determine the upper limit of $|F|$ which will yield the lower limit of k_{ex} from Eq 6b.

For a given $\tilde{k}_{ex}$ reaches its maximum value at $|t|=1$. In reality, as can be seen from Figure 2, $\tilde{k}_{ex}$, is somewhat dependent on r. Nonetheless, it can be shown that taking this indirect dependence into account does not change the conclusion that $|F|$ reaches its maximum at $|t|=1$. Thus,

$$\max|F| = \frac{\tilde{k}_{ex}^2}{\left(1+\tilde{k}_{ex}^2\right)^2 - 1} = \frac{1}{2+\tilde{k}_{ex}^2}, \quad (9)$$

where the value of $\tilde{k}_{ex}$ has to be obtained from the ratio of F factors taking $|t|=1$. For small values of $\tilde{k}_{ex}$, the ratio of $R_{CSM/CSM}$ at two fields depends rather dramatically on r^2, which has little practical interest as $R_{CSM/CSM}$ terms become negligibly small in this limit.

Within the assumption above of $p_1 \gg p_2$, it is reasonable to take the maximum of $p_1p_2=0.2$, which corresponds to 30% of the minor population. Then the lower limit of k_{ex} can be calculated as

$$\min k_{ex} = \left|R_{CSM/CSM}\right|/(0.2 \max|F|) \quad (10)$$

Note, than $R_{CSM/CSM}$ can be taken at either of the two fields.

III. Example of relative strengths of R_{ex} contributions in SQ and MQ coherences for the same motional process—A detailed analysis of relative strengths of R_{ex} terms for SQ and MQ coherences (involving one of the nuclei in the SQ coherence) under the assumption of the same motional processes contributing to the two coherences has been performed by Wang and Palmer (Wang and Palmer 2002) and Korzhnev et al. (Korzhnev et al. 2004). For the $^{15}N-^{13}C'$ experiment, in the fast exchange limit, the ratio of ^{15}N SQ R_{ex} term to $R_{CSM/CSM}$ is given by $\left|R_{ex}/R_{CSM/CSM}\right| = 0.5\left|\Delta\omega_N/\Delta\omega_{C'}\right|$. Thus, the $\Delta\omega_N/\Delta\omega_{C'}$ ratio defines the relative effectiveness of using R_{ex} or $R_{CSM/CSM}$ in detecting the motional process. If the exchange is not in the fast regime, the ratio $\Delta\omega_N/\Delta\omega_{C'}$ is still a

determining factor with the dependence becoming more complex, as can be calculated using Eqs. (6 & 7). Figure 3A demonstrates the condition on this ratio in order for the $R_{CSM/CSM}$ term to exceed the R_{ex} term for threshold levels between 5 and 30%. The example is shown as a function of the ratio of $R_{CSM/CSM}$ at two field strength values of 900 and 500 MHz.

To demonstrate its application to a specific case related to our experimental $^{13}C—^{15}N$ data at two fields of 500 and 900 MHz, we also explicitly show $R_{ex}/R_{CSM/CSM}$ for a $R_{CSM/CSM}$ (900 MHz)/ $R_{CSM/CSM}$(500 MHz) ratio of 2.7 as a function of $\Delta\omega_N/\Delta\omega_{C'}$. The results, shown in Figure 3B, indicate that when $\Delta\omega_N < 0.18\ \Delta\omega_{C'}$, R_{ex} is expected to be under 10% of $R_{CSM/CSM}$

IV. Calculations of "unwanted" dipolar and CSA contributions.—The dipolar contributions can be calculated using the following expression:

$$R_{DD/DD} = \sum_k R_{DD/DD}(AX_k/BX_k), \quad (11)$$

where each term in the sum gives the contribution to the relaxation rate from two dipole-dipole mechanisms involving spin A, B, and any other nucleus in a protein, denoted by X_k. Under the assumption of the slow tumbling limit and fast internal motions, each $R_{DD/DD}$ rate in the sum is calculated as:

$$R_{DD/DD}(AX_k/BX_k) = \left(\frac{\mu_0\hbar}{4\pi}\right)^2 \frac{2\tau_c}{5} \frac{\gamma_A\gamma_B\gamma_{X_k}^2}{r_{AX_k}^3 r_{BX_k}^3} P_2(\cos\theta_k) S^2_{DD/DD,k} \quad (12)$$

where μ_0 is the permeability of free space, and γ_A, γ_B, γ_{X_k} are the gyromagnetic ratios. τ_c is the correlation time for molecular tumbling, r_{AX_k} and r_{BX_k} are distances of dipole-dipole interactions, θ_k is the angle between AX_k and BX_k vectors, P_2 is the second rank Legendre polynomial and $S^2_{DD/DD,k}$ is the order parameter describing the amplitude of the fluctuations of these interactions. The distances and the angles are calculated from known GB3 structural coordinates, taken from the originally RDC-refined X-ray structure 2OED (Ulmer et al. 2003), which was further refined with additional RDCs (Yao et al. 2008a; Yao et al. 2008b). The effect of deuteration has to be taken into account for non-exchangeable protons. In the deuterated protein, dipolar contributions are largely reduced by a factor of about 42 due to the significantly reduced gyromagnetic ratio of deuterons: $(\gamma_H/\gamma_D)^2$=42. This reduction is considerably more dramatic for the $C_\alpha C_\beta$ relaxation rates because in the deuterated protein all neighboring protons are replaced by deuterons. In the case of C'N the amide proton provides a dominant contribution in both protonated and deuterated proteins. In Eq. 12, we assume fast motion only. This assumption may not be valid for long-range DD/DD contributions. However, this deviation is expected to have a negligible effect due to very small contributions from these long-ranged interactions.

In order to account for the dynamics effects of fast motions, the following values for the order parameters are used in this work, which represent typical values encountered in globular proteins (Cavanagh et al. 2006; Yang et al. 1998): For all backbone interactions in the C'N experiment $S^2_{DD/DD,k}$ was taken as 0.8. In the $C_\alpha C_\beta$ case, a value of 0.8 was used for all interactions involving H_α or D_β and for all interactions involving an external nucleus. For the case of interactions involving H_α or D_β a value of 0.5 was employed. Deviations from these values introduce a relatively minor source of error into $R_{CSM/CSM}$ rates, and therefore they do not change the overall conclusions of the work and are discussed in more detail in the *Experimental Results* section and Online Resource SI1.

Calculation of the $R_{CSA/CSA}$ rates requires knowledge of the tensor components.—For C_α and C_β, axial symmetry is assumed. Asymmetry parameters for C_α nuclei were estimated as 27± 4.3 ppm for β-sheets and 6.1± 4.9 for α-helices. For C_β nuclei, the asymmetry parameters were measured for amino acids in the solid state, yielding a wide range of 18–45 ppm (Tjandra and Bax 1997; Ye et al. 1993). Thus, the upper limit of the C_α/C_β CSA/CSA interaction can be approximated by taking the parallel orientation of the two tensors with the asymmetries of 30 ppm for C_α and 45 ppm for C_β. This yields the upper limit on the values around 0.76 s^{-1} for protonated GB3 at 500 MHz and 2.5 s^{-1} at 900 MHz.

Since $^{13}C'$ CSA tensors have a strong rhombicity (Tang and Case 2007), one has to take into account all of the components of the CSA tensor. ^{15}N tensors can also have a substantial extent of rhombicity, based on previous studies (Loth et al. 2005; Yao et al. 2010). The components of the ^{15}N and $^{13}C'$ CSA tensors were estimated using the empirical rules derived by Loth *et al.* (Loth et al. 2005) from sets of auto- and crosscorrelated relaxation rates in ubiquitin. These empirical rules allow the calculations of the fully anisotropic CSA tensor components (denoted by σ_{ii}) from the values of isotropic chemical shift based on the specific motional models. We have chosen the following tensor components: (Kateb et al. 2006) $\sigma_{zz}{}^C$=83.6ppm, $\sigma_{xx}{}^C$=251.2 ppm and $\sigma_{yy}{}^C = 3\sigma_{iso}{}^C - 334.9$ ppm for C′ and $\sigma_{zz}{}^N$= 57.7 ppm, $\sigma_{xx}{}^N = \sigma_{iso}{}^N + 105.5$ppm and $\sigma_{yy}{}^N = 2\sigma_{iso}{}^N - 163.2$ ppm for ^{15}N. Here σ_{iso} stands for the isotropic chemical shift. Internal fast motions were approximated with an order parameter of 0.8 for all interactions. The expressions for the $R_{CSA/CSA}$ term are obtained in an analogous fashion to the dipolar contribution and are given in SI2. All isotropic chemical shifts for GB3 except for carbonyl carbons were reported previously (pdb/bmrb entry 2LUM) (Vogeli et al. 2012). C' chemical shifts were obtained from a 3D HNCO experiment (SI3). It is of note that Yao et al.(Yao et al. 2010) have derived a somewhat different set of rules for ^{15}N CSA tensors of GB3 based on the isotropic chemical shift, resulting from the analysis of six mutants in several liquid crystalline alignment media. The resulting differences between the $^{13}C'/^{15}N$ CSA/CSA term obtained from the rules of Loth et al. and Yao et al. are small, with the average value over all residues of —0.08 s^{-1} and a standard deviation of 0.1 s^{-1}. Additionally, Hall and Fushman (Hall and Fushman 2006) have obtained a detailed description of ^{15}N CSA tensors from a number of auto- and cross-relaxation rates at several magnetic field values. This analysis was performed under the assumption of axial symmetry of the ^{15}N CSA tensors. A typical per residue variability in the anisotropy was on the order of 20 ppm, which is less than 10% variation. (The average

anisotropy was calculated between (—173) and (—177) ppm for a 1.02 Å NH bond length). The rules of Loth et al. to calculate the effective anisotropy yield the same anisotropy of —158 ppm for all residues. All different estimates of anisotropy appear to be within 10% variability in their effect on the $^{13}C'/^{15}N$ CSA/CSA term.

The CSA changes for ^{15}N and $^{13}C'$ nuclei upon deuteration are expected to be negligible based on maximum possible chemical shift differences reported by Maltzev et al. (Maltsev et al. 2012) and Venters et al. (Venters et al. 1996). The effect of deuteration on chemical shift anisotropy of C_α and C_β could be more substantial, but is most likely well within the uncertainties of the actual asymmetry values as well as within the experimental error bars of the differential rate, ΔR.

V. Scalar coupling to aliphatic C_γ carbons and the effect of longer-range couplings.—As mentioned above, the decay curves of ZQ and DQ coherences in the case of C_α— C_β are modulated by scalar coupling to aliphatic C_γ nuclei according to $(\cos \pi J_{eff} \tau)^n$, in which n is the number of the aliphatic C_γ carbons, and τ is the variable relaxation time. The effective couplings J_{eff} are given by:

$$^{ZQ}J_{eff} = {}^1J\left(C_\beta C_\gamma\right) - {}^2J\left(C_a C_\gamma\right) \text{ and } {}^{DQ}J_{eff} = {}^1J\left(C_\beta C_\gamma\right) + {}^2J\left(C_a C_\gamma\right) \quad (13)$$

Thus, from the sums and the differences of these effective couplings one can obtain the values of $^1J(C_\beta C_\gamma)$ and $2J(CaC\gamma)$.

Longer-range couplings are not included in our treatment. To estimate the effect of the additional longer-range coupling that affect differentially the DQ and ZQ coherences, such as couplings to C_δ nuclei, one can perform simulations with typical values of R_{DQ}, R_{ZQ} of about 60 s^{-1}, $J_{\beta\gamma}$ of 35 Hz, $J_{a\gamma}$ of 3 Hz, $J_{\beta\gamma}$ of 3 Hz, and $J_{\alpha\delta}$ of 1 Hz (i.e., maximum expected value for the last two couplings). The extra modulation manifests as an additional drop in intensity and effectively changes relaxation rates and not the J-coupling constant. In the following results we used a maximum experimental relaxation delay of 50 ms. The magnitude of the rate increase is 2.3 s^{-1} for the CACB R_{DQ} rate and 0.6 s^{-1} for the R_{ZQ}, thus its effect on ΔR is up to 0.9 s^{-1}. Longer-range modulations that affect both coherences equally, such as $J_{C'(i)—C'(i+1)}$ coupling for the C'N MQ coherences, do not cause a net effect on the magnitude of ΔR. We also note that introducing two different coupling constants for two different C_γ carbons is outside the expected precision of the data.

Experimental Results

Several examples of decay curves are shown in Figure 4. Note that in the C'N experiment the differential rate ΔR, defined in Eq. 1, was determined from fitting the ratio of intensities from the DQ and ZQ spectra as a function of delay time (Figure 4A). Fitting the ratio results in the removal of any potential systematic errors that might be present for both the DQ and ZQ decays. This approach is not feasible for the CACB case due to the presence of scalar coupling to aliphatic C_γ nuclei. Thus, the fits, examples of which are shown in Figure 4B, were performed individually for the R_{DQ} and R_{ZQ} rates.

ΔR rates are shown in Figure 5 for both protonated and deuterated proteins at two magnetic field strengths, 500 and 900 MHz (11.7 and 21.1 T). Among the terms specified in Eq. 2, the DD/DD terms as approximated in Eq. 12 are field independent, while both CSA/CSA and CSM/CSM can contribute to field dependence. Deuteration significantly reduces the DD/DD terms involving non-exchangeable protons due to differences in the gyromagnetic ratio of proton and deuteron, but to the first approximation does not affect CSA/CSA interference (see theory section). Deuteration could affect CSM/CSM contributions through its potential effect on slow motions. Visual representation of DD/DD and CSA/CSA contributions to ΔR rates are shown in SI4 and a table of values is given in SI5.

I. Concerted motions of backbone ^{13}C' and ^{15}N nuclei.—To obtain the CSM/CSM contributions, which reflect most directly the correlated slow motions of the two nuclei, one has to subtract the "unwanted" dipolar and CSA terms (Eq, (2)). As elaborated above, there are quite a number of assumptions involved in these calculations, however, they only affect the estimate of the "unwanted" terms up to ~ 10%. The effect of the variability of the backbone order parameters for the fast internal motions that affect the $R_{\mathrm{DD/DD}}$ and $R_{\mathrm{CSA/CSA}}$ terms is further analyzed in SI1. The main conclusions are not affected by these uncertainties.

Values of $R_{\mathrm{CSM/CSM}}$ calculated under these assumptions are shown in Figure 5, panels C&D, for the two fields and both protonated and deuterated proteins. There is an overall good correlation between the data at the two fields and the two proteins (Figure 5 and SI6). For the N-terminal residues of GB3 (residues 3–15), CSM/CSM contributions are relatively minor. For these residues the values are close to zero at 500 MHz and they display a mixture of positive and negative rates at 900 MHz, with a tendency towards positive values of $R_{\mathrm{CSM/CSM}}$. Note that a positive $R_{\mathrm{CSM/CSM}}$ value means anti-correlated motions for the C'—N pairs, and negative values indicate correlated motions. In the range of residues 20–40, CSM/CSM contributions are significant and there is a tendency towards negative $R_{\mathrm{CSM/CSM}}$ rates. For the range of 41–55 there is again of mixture of positive and negative rates. Residue 54 has a very large positive $R_{\mathrm{CSM/CSM}}$ rate of 9 s^{-1} at 900 MHz. Thus the rates suggest correlated motions in the α-helical region (residues 22–37), which might indicate that the atoms move in the same direction that causes shielding/deshielding. No regularities are discerned for the β-sheet regions. Of note, there is a relatively small but consistent trend for the C'—N $R_{CSM/CSM}$ values of many of the residues to be smaller in the deuterated protein (Figure 5 and S7), implying that there is a possibility of deuteration reducing some of the motions.

The field dependence of the data can put constraints on the chemical shift time scales of the motions. Within the errors of the measurements and all of the assumptions that go into calculating the "unwanted" terms, residue-specific values may not be reliable, but a weighted average over all data should provide a relatively robust estimate of this effect. To calculate the average field dependence of the rates, we analyzed the correlations of ΔR and $R_{CSM/CSM}$ at the two fields. The slopes (shown in the right-hand corner of the Figure 6 plots) represents the field dependence of either the combined $R_{\mathrm{CSA/CSA}} + R_{CSM/CSM}$ contributions in the case of ΔR correlations because the $R_{\mathrm{DD/DD}}$ terms are the same for the two fields or only CSM/CSM contributions in the case of $R_{CSM/CSM}$ correlations. Note that

the field dependence of the CSA/CSA term alone is expected to scale quadratically with the fields, while the field dependence of $R_{CSM/CSM}$ is governed by the time scale of motions.

The slopes for the correlations of the $R_{CSM/CSM}$ terms are around 2.7, which, using the results of Figure 2, $\tilde{k}_{ex} = \frac{k_{ex}}{\sqrt{\Delta\omega_N^2 + \Delta\omega_{C'}^2}}$ puts the ratio at 4.6 (i.e, intermediate to fast regime), regardless of the values of the relative chemical shift differences $\Delta\omega_N$ and $\Delta\omega_{C'}$, expressed through the value of r^2. Using these constraints along with the typical maximum chemical shift changes specified in the theoretical section, one obtains an upper limit on the k_{ex} value of 430 s^{-1}. Using the approach explained in the theoretical section, the lower limit on the k_{ex} value can be obtained from Eqs. 9 and 10, which yields max|F|=0.045 and, thus, the lower limit of k_{ex} is about 200 s^{-1} for residues with the maximum CSM/CSM contributions (i.e., —1.8 s^{-1} at 500 MHz) and for moderate CSM/CSM contributions (around —1.0 s^{-1} at 500 MHz) it is 110 s^{-1}.

The nonzero $R_{CSM/CSM}$ values for many residues imply extensive concerted slow fluctuations of the C' and N nuclei. Yet SQ chemical exchange measurements on ^{15}N nuclei did not detect slow motions for most residues.(Hall and Fushman 2006) This means that either C'—N correlations involve additional motions not sensed by the N—H bond vectors alone, as is in principle possible based on the differences in the dynamics between ^{15}N and ^{13}C' nuclei. (Vugmeyster and Ostrovsky 2011; Vugmeyster et al. 2010; Wang et al. 2003; Wang et al. 2005), or the interplay of the rate constant and chemical shifts differences is such that the motions that are detected by the MQ experiments are obscured in the SQ measurements. A detailed analysis of the latter option is given in the theoretical section (Figure 3B). The results indicate the following constraints on the relative chemical shifts differences in order for R_{ex} to be under 10% of $R_{CSM/CSM}$ at the fixed ratio $R_{CSM/CSM}$ at 900/ $R_{CSM/CSM}$ at 500 = 2.7: $\Delta\omega_N < 0.18\Delta\omega'_C$. If this condition holds, then with the typical value of $R_{CSM/CSM}$ at around 3 s^{-1} (Figure 5), the expected R_{ex} contributions are under 0.3 s^{-1} and are not easily detected. Interestingly, in the SQ ^{15}N measurements at the 800 MHz field strength (Hall and Fushman 2006), in which a standard CPMG-refocusing procedure was employed for the R_2 measurements, 13 residues have displayed non-zero R_{ex} contributions when fitted with the extended Lipari-Szabo modelfree approach.(Clore et al. 1990) However, for all of them, other than Val39, the contributions were marginal, with the maximum around 0.5 s^{-1}, which is right at the detection limit suggested by the above analysis. Very careful ^{15}N and ^{13}C' SQ measurements with a single echo period in the relaxation block could potentially distinguish between the two scenarios of small ^{15}N SQ R_{ex} term versus additional motions of the C'—N bond vector.

II. Correlated motions of $^{13}C_\alpha$—$^{13}C_\beta$ pairs and differences between protonated and deuterated proteins—ΔR rates for $^{13}C_\alpha$—$^{13}C_\beta$ pairs in the protonated protein display a good agreement between the two fields (Figure 7A and8). The comparison between the protonated and deuterated proteins (Figure 7 and SI6) indicates a marked overall reduction in the rates upon deuteration. The most obvious cause of the reduction is the scaling by a factor of 1/42 of all dipolar terms that involve two non-exchangeable protons, which are the major source of the DD/DD contributions in Eq.2. Note this is in

contrast to the dipolar contributions in the C'—N case. However, when the dipolar contributions are subtracted from the experimental ΔR rates, according to the calculations described in the theory section, the resulting rates, $\Delta R - R_{DD/DD}$, are still very different between the protonated and deuterated proteins. Assuming comparable CSA/CSA terms, (albeit scaled with the different tumbling times), this residual reduction likely originates from the diminished CSM/CSM term in the deuterated proteins. We do not show calculated $R_{\mathrm{CSM/CSM}}$ rates on the per residues basis because of the large uncertainties associated in the calculations of $^{13}C_\alpha/^{13}C_\beta$ $R_{\mathrm{CSA/CSA}}$ term, stemming from the uncertainties in the values of $\Delta\sigma c_\beta$ (see the theory section above) and relative orientations of the $^{13}C_\alpha$ and C_β CSA tensors. The upper limit of this term for the protonated protein is on the order of 0.75 s^{-1} for the 500 and 2.5 s^{-1} for the 900 MHz field, if the values of the order parameters for fast motions are taken as 1 and one assumes parallel tensor orientation and the maximum values of the anisotropies. The typical values of the $R_{\mathrm{CSA/CSA}}$ terms are likely half of these maximum contributions at most due to smaller anisotropy values, non-parallel relative tensor orientation, and reduction through the true fast motion order parameter.

As $\Delta R - R_{DD/DD}$ rates are close to zero for most residues in the deuterated protein, we assume to a first approximation that there are almost no slow concerted motions in the deuterated protein. Thus, the values of $\Delta R - R_{DD/DD}$ for the deuterated protein could be used as rough baseline containing primarily the "unwanted" CSA/CSA interactions. Under these assumptions, the $R_{\mathrm{CSM/CSM}}$ values in the protonated protein can be calculated as

$$R_{CSM/CSM} = \left(\Delta R - R_{DD/DD}\right)_{prot} - \left(\Delta R - R_{DD/DD}\right)_{deut} \quad (14)$$

There is a mixture of positive and negative $\Delta R - R_{DD/DD}$ and $R_{\mathrm{CSM/CSM}}$ values in the protonated protein (Figure 9), and no particular correlation to specific secondary structure elements is observed. Of particular note, in regards to larger CSM/CSM contributions, are clusters of side-chains in relative proximity to each other: VAL39-VAL54-LEU5 and possibly ALA20-TYR3-ALA23 (Figure 10). In addition, there are a number of relatively solvent-exposed side-chains that show significant CSM/CSM contributions: LYS4, ASN8, THR11, VAL21, ASP22, GLU27, LYS28, GLN32, ASP36, ASP46, and LYS50. Thus, based on this clustering analysis, it appears that the CSM/CSM measurements report on local structural rearrangements, possibly arising due to local unfolding events. Smith et al. (Smith et al. 2015) have also detected population shuffling of rotameric states by high power relaxation dispersion measurements (sensitive to motions as fast as 3–9 μs) at ^1H and $^{13}C_\gamma$ sites of several methyl groups in GB3. Out of the residues exhibiting significant $C_\alpha C_\beta$ CSM/CSM contributions, which are on a much slower time scale of 0.01 s, L5, V21, and V54 have also been identified as undergoing this population shuffling.

The values of $^1J(C_\beta C_\gamma)$and $^2J(C_aC_\gamma)$ were obtained from experimental values of $^{ZQ}J_{eff}$ and $^{DQ}J_{eff}$ according to Eq. 13 (Figure 11). In general, they do not exhibit any systematic differences between the protonated and deuterated proteins, indicating no significant overall structural changes. There are a few residues that show some deviations between the two samples (Figure 11 and SI7), such as 4, 13, 18, 28, 32, 44, 50, and 53, suggesting

possibilities of local structural variations upon deuteration. To further check the influence of the J-coupling constants on the fitted values of rates ΔR, we performed a fit for the protonated protein at 500 MHz in which the values $^1J(C_iC_\gamma)$ of the J-coupling constants were fixed at the average values obtained for the protonated and deuterated proteins (SI8). The effect on the resulting values of ΔR is small, with an increase in the error bars, as expected. In principle, the J-coupling constants are expected to be field-independent and a joint fit of the relaxation decay curves can be performed for the two fields. However, in practice these parameters appear to be particularly sensitive to any residual systematic errors between the two spectrometers and, thus, a joint fit is expected to compromise the precision of the resulting ΔR values.

As was described in the theory section and done with the C'—N measurements, it is possible to obtain constraints on the upper limit of k_{ex} using the field dependence of the data and expected typical maximal variations in the values of the chemical shifts $\Delta\omega_{C\alpha}$ and $\Delta\omega_{C\alpha}$. The correlation plot of ΔR —$R_{DD/DD}$ at the two fields yields a value of 1.7 for the protonated protein, whereas the one for the two fields for the $R_{CSM/CSM}$ yields the value of 1.6 (Figure 8). With these values and the analysis depicted in Figure 2, $\tilde{k}_{ex} = \frac{k_{ex}}{\sqrt{\Delta\omega_{c_\alpha}^2 + \Delta\omega_{c_\beta}^2}}$ is constrained to a range of 1.5–2.0 and the maximum value of k_{ex} is then 160 s^{-1} . The lower limit of k_{ex} is again estimated using Eqs. 9 and 10, yielding max|F|=0.23 at 500 MHz and k_{ex} of 100 s^{-1} for average values of $R_{CSM/CSM}$. Thus, the typical value of k_{ex} is around 100—160 s^{-1}.

Further studies are needed to investigate if deuteration indeed causes changes in the slow concerted dynamics, especially at the nuclei which are part of the perdeuterated network. It is unlikely that these extensive differences in the C_α—C_β motions between the protonated and deuterated proteins are caused by oligomeric exchange in the more concentrated protonated GB3 sample, as GB3 protein is known to be monomeric at high concentrations and other NMR studies using up to 4 mM concentration have been published (Vögeli and Yao 2009). Further, if extensive oligomeric exchange were present, it would likely be also seen in the C'—N measurements, unless the chemical shift difference between monomers and oligomers is very small.

It has been shown in a number of studies that deuteration at non-exchangeable sites can cause a modest but measurable reduction in protein stability ((Piszczek et al. 2011) and references therein, (Hattori et al. 1965)). The effect of deuteration is different from solvation of proteins in D_2O, which has long been known to enhance protein stability over H_2O due to differences in H-bond length and polarization (Maybury and Katz 1956). Additionally, it was found that in D_2O proteins tend to be more rigid (Cioni and Strambini 2002). The nature of the isotope effect on *non-exchangeable* aliphatic and aromatic groups is fundamentally different and not widely appreciated. Data on small molecules (Turowski et al. 2003) suggests that the main effect of deuteration may be changes in the van der Waals forces due to reduced vibrations of deuterons compared to protons. A number of studies indicate that deuteration also causes changes in dynamics, catalytic activity, ligand binding, and oligomerization ((Brockwell et al. 2001; Piszczek et al. 2011; Venters et al. 1996; Yee et al.

2016) and references therein). Whether the dynamical processes are enhanced or suppressed by deuteration of non-exchangeable groups appears to depend on the protein as well as on the specifics of the time scales and mechanisms of the motional mode investigated. A hint of possible changes of correlated motions of C_α and C_β nuclei upon deuteration has previously been observed for ubiquitin. (Vugmeyster et al. 2004). However, the magnitude of the experimental errors in the measurements for the protonated protein prohibited a quantitative support of this conclusion. Interestingly, for one of the key residues (Y54) in Fyn G48M SH3 domain, relaxation dispersion measurements involving ^{1}H, ^{15}N SQ and ^{1}H— ^{15}N MQ coherences indicated that population of the unfolded state and the folding rate are reduced upon deuteration, pointing to a reduction in stability of the folded state. (Korzhnev et al. 2004)

The two GB3 proteins show different reversed-phase HPLC retention times (Figure 12). The deuterated protein elutes first, which suggests decreased hydrophobicity, potentially arising from altered van der Waals forces in response to the reduced vibrations expected from the higher mass of deuterium.

Conclusions

We have demonstrated that cross-correlated chemical shift modulation measurements combined with the field dependence can be very effective in identifying slow concerted fluctuations of backbone and sidechain nuclei. The majority of residues in GB3 displayed the presence of concerted fluctuations in the backbone C'—N nuclei, with the typical time scale of 110–430 s^{-1}. As SQ ^{15}N measurements on GB3 did not show significant R_{ex} contributions for most residues in previously published studies (Hall and Fushman 2003; Hall and Fushman 2006), an analysis was performed to determine the relative chemical shift differences $\Delta\omega_N$ and $\Delta\omega_{C'}$ that would be required to largely obscure motions in the SQ measurements, under the assumption of the same motional processes for the ^{15}N—H and ^{13}C'—^{15}N bond vectors. The condition was found to be $\Delta\omega_N < 0.18\Delta\omega_{C'}$. Many residues also revealed slow concerted fluctuations in $^{13}C_\alpha$— $^{13}C_\beta$ pairs and the field-dependence has permitted us to constrain the typical value of k_{ex} to about 100–150 s^{-1}. On average, backbone motions fell into the intermediate to fast regime, while the side-chain motions were close to the slow to intermediate regime on the chemical shift time scales. Many assumptions had to be made in order to calculate the $R_{CSM/CSM}$ terms, which include taking distances from structural coordinates, educated guesses on the order parameters for the fast motions, assumptions regarding CSA tensor components, and the assumption of isotropic tumbling. The CSA tensor components for C_β nuclei are not well known, and further assumptions had to be made to extract the CSM/CSM contributions. Thus, the extracted values of $R_{CSM/CSM}$ for individual residues are not exact. However, combining data for all residues, they provide a good measure of the overall qualitative picture of motions.

Deuteration causes a drastic, 42-fold reduction in the dipolar contributions to the relaxation of the C_α—C_β MQ coherences, thus reducing the "unwanted" terms. The impact of deuteration on dipolar terms is smaller for the backbone C'—N coherences because the major interaction involves the amide protons, which are solvent-exchangeable and

protonated in both proteins. An interesting implication of this study is a possible effect of deuteration on the slow concerted motions. While the effect is relatively small for the C'—N backbone pairs, it is rather pronounced for the C_α—C_β pairs, which are part of the perdeuterated network, with an apparent reduction in $R_{CSM/CSM}$ values in the deuterated sample. Further studies are needed to investigate this effect.

Supplementary Material

Refer to Web version on PubMed Central for supplementary material.

Acknowledgements

This work has been supported by National Institutes of Health Grant 1R15-GM111681 to L.V, Research Corporation PUI-R1 Partnership Award to L.V. and C.J.M., NIH grant S10OD011941 to C.J.M, and a startup package from the University of Colorado at Denver to B.V. Some of the work presented here was conducted at the Center on Macromolecular Dynamics by NMR Spectroscopy located at the New York Structural Biology Center, supported by a grant from the NIH National Institute of General Medical Sciences (P41 GM118302) and ORIP/NIH facility improvement grant CO6RR015495. The 900 MHz NMR spectrometers were purchased with funds from NIH grant P41GM066354, the Keck Foundation, New York State Assembly, and U.S. Dept. of Defense. We thank Robert Hodges at CU Denver Anschutz Medical Campus for access to analytical HPLC equipment.

References

Arnold WD, Oldfield E (2000) The chemical nature of hydrogen bonding in proteins via NMR: Jcouplings, chemical shifts, and AIM theory. J Am Chem Soc 122:12835–12841

Brockwell D et al. (2001) Physicochemical consequences of the perdeuteriation of glutathione Stransferase from S. japonicum. Prot Sci 10:572–580

Brutscher B, Skrynnikov NR, Bremi T, Bruschweiler R, Ernst RR (1998) Quantitative investigation of dipole-CSA cross-correlated relaxation by ZQ/DQ spectroscopy. J Magn Reson 130:346–351 [PubMed: 9500898]

Cavanagh J, Fairborther WJ, Palmer AGP, Skelton NJ, Rance M (2006) Protein NMR Spectroscopy Principles and Practice. 2nd ed. Elsevier Academic Press

Cioni P, Strambini GB (2002) Effect of heavy water on protein flexibility. Biophys J 82:3246–3253 [PubMed: 12023248]

Clore GM, Szabo A, Bax A, Kay LE, Driscoll PC, Gronenborn AM (1990) Deviations from the simple 2-parameter model-free approach to the interpretation of N-15 nuclear magnetic-relaxation of proteins. J Am Chem Soc 112:4989–4991

Delaglio F, Grzesiek S, Vuister GW, Zhu G, Pfeifer J, Bax A (1995) NMRPipe: a multidimensional spectral processing system based on UNIX pipes. J Biomol NMR 6:277–293 [PubMed: 8520220]

Derrick JP, Wigley DB (1994) The third IgG-binding domain from streptococcal protein G. An analysis by X-ray crystallography of the structure alone and in a complex with FAB. J Mol Biol 243:906918

Frueh D (2002) Internal motions in proteins and interference effects in nuclear magnetic resonance. Prog Nucl Magn Reson Spectrosc 41:305–324

Fruh D, Tolman JR, Bodenhausen G, Zwahlen C (2001) Cross-correlated chemical shift modulation: a signature of slow internal motions in proteins. J Am Chem Soc 123:4810–4816 [PubMed: 11457291]

Hall JB, Fushman D (2003) Characterization of the overall and local dynamics of a protein with intermediate rotational anisotropy: Differentiating between conformational exchange and anisotropic diffusion in the B3 domain of protein G. J Biomol NMR 27:261–275 [PubMed: 12975584]

Hall JB, Fushman D (2006) Variability of the N-15 chemical shielding tensors in the B3 domain of protein G from N-15 relaxation measurements at several fields. Implications for backbone order parameters. J Am Chem Soc 128:7855–7870 [PubMed: 16771499]

Hattori A, Crespi HL, Katz JJ (1965) Effect of side-Chain deuteration on protein stability. Biochemistry 4:1213–1225 [PubMed: 5856627]

Iwadate M, Asakura T, Williamson MP (1999) C alpha and C beta carbon-13 chemical shifts in proteins from an empirical database. J Biomol NMR 13:199–211 [PubMed: 10212983]

Kateb F, Abergel D, Blouquit Y, Duchambon P, Craescu CT, Bodenhausen G (2006) Slow backbone dynamics of the C-terminal fragment of human centrin 2 in complex with a target peptide probed by cross-correlated relaxation in multiple-quantum NMR spectroscopy. Biochemistry 45:1501115019

Kay LE, Ikura M, Tschudin R, Bax A (1990) Three-dimensional triple-resonance NMR spectroscopy of isotopically enriched proteins. J Magn Reson 89:496–514

Korzhnev DM, Kloiber K, Kay LE (2004) Multiple-quantum relaxation dispersion NMR spectroscopy probing millisecond time-scale dynamics in proteins: theory and application. J Am Chem Soc 126:7320–7329 [PubMed: 15186169]

Lakomek NA, Ying J, Bax A (2012) Measurement of (1)(5)N relaxation rates in perdeuterated proteins by TROSY-based methods. J Biomol NMR 53:209–221 [PubMed: 22689066]

Le H, Oldfield E (1994) Correlation between 15N NMR chemical shifts in proteins and secondary structure. J Biomol NMR 4:341–348 [PubMed: 8019141]

Lee D, Hilty C, Wider G, Wuthrich K (2006) Effective rotational correlation times of proteins from NMR relaxation interference. J Magn Reson 178:72–76 [PubMed: 16188473]

Loth K, Pelupessy P, Bodenhausen G (2005) Chemical shift anisotropy tensors of carbonyl, nitrogen, and amide proton nuclei in proteins through cross-correlated relaxation in NMR spectroscopy. J Am Chem Soc 127:6062–6068 [PubMed: 15839707]

Lundstrom P, Akke M (2004) Quantitative analysis of conformational exchange contributions to 1H-15N multiple-quantum relaxation using field-dependent measurements. Time scale and structural characterization of exchange in a calmodulin C-terminal domain mutant. J Am Chem Soc 126:928–935 [PubMed: 14733570]

Lundstrom P, Mulder FA, Akke M (2005) Correlated dynamics of consecutive residues reveal transient and cooperative unfolding of secondary structure in proteins. Proc Natl Acad Sci U S A 102:16984–16989 [PubMed: 16278300]

Majumdar A, Ghose R (2004) Probing slow backbone dynamics in proteins using TROSY-based experiments to detect cross-correlated time-modulation of isotropic chemical shifts. J Biomol NMR 28:213–227 [PubMed: 14752255]

Maltsev AS, Ying J, Bax A (2012) Deuterium isotope shifts for backbone (1)H, (15)N and (13)C nuclei in intrinsically disordered protein -synuclein. J Biomol NMR 54:181–191 [PubMed: 22960996]

Maybury RH, Katz JJ (1956) Protein denaturation in heavy water. Nature 177:629–630

Millet O, Loria JP, Kroenke CD, Pons M, Palmer AG (2000) The static magnetic field dependence of chemical exchange linebroadening defines the NMR chemical shift time scale. J Am Chem Soc 122:2867–2877

Pellecchia M, Pang YX, Wang LC, Kurochkin AV, Kumar A, Zuiderweg ERP (1999) Quantitative measurement of cross-correlations between N-15 and (CO)-C-13 chemical shift anisotropy relaxation mechanisms by multiple quantum NMR. J Am Chem Soc 121:9165–9170

Perazzolo C, Wist J, Loth K, Poggi L, Homans S, Bodenhausen G (2005) Effects of protein-pheromone complexation on correlated chemical shift modulations. J Biomol NMR 33:233–242 [PubMed: 16341752]

Piszczek G, Lee JC, Tjandra N, Lee CR, Seok YJ, Levine RL, Peterkofsky A (2011) Deuteration of Escherichia coli enzyme I(NTR) alters its stability. Archives of biochemistry and biophysics 507:332–342 [PubMed: 21185804]

Smith CA et al. (2015) Population shuffling of protein conformations. Angew Chem Int Ed 54:207–210

Tang S, Case DA (2007) Vibrational averaging of chemical shift anisotropies in model peptides. J Biomol NMR 38:255–266 [PubMed: 17562185]

Tjandra N, Bax A (1997) Large variations in C-13(alpha) chemical shift anisotropy in proteins correlate with secondary structure. J Am Chem Soc 119:9576–9577

Turowski M et al. (2003) Deuterium isotope effects on hydrophobic interactions: the importance of dispersion interactions in the hydrophobic phase. J Am Chem Soc 125:13836–13849 [PubMed: 14599224]

Ulmer TS, Ramirez BE, Delaglio F, Bax A (2003) Evaluation of backbone proton positions and dynamics in a small protein by liquid crystal NMR spectroscopy. J Am Chem Soc 125:9179–9191 [PubMed: 15369375]

Venters RA, Farmer BT, 2nd, Fierke CA, Spicer LD (1996) Characterizing the use of perdeuteration in NMR studies of large proteins: 13C, 15N and 1H assignments of human carbonic anhydrase II. J Mol Biol 264:1101–1116 [PubMed: 9000633]

Vogeli B, Kazemi S, Guntert P, Riek R (2012) Spatial elucidation of motion in proteins by ensemblebased structure calculation using exact NOEs. Nat Struct Mol Biol 19:1053–1057 [PubMed: 22940676]

Vögeli B, Yao L (2009) Correlated dynamics between protein HN and HC bonds observed by NMR cross relaxation. J Am Chem Soc 131:3668–3678 [PubMed: 19235934]

Vögeli B, Yao L, Bax A (2008) Protein backbone motions viewed by intraresidue and sequential HN–Hα residual dipolar couplings. J Biomol NMR 41:17 [PubMed: 18458825]

Vugmeyster L (2009) Slow backbone dynamics of chicken villin headpiece subdomain probed by NMR C-N cross-correlated relaxation. Magn Reson Chem 47:746–751 [PubMed: 19479944]

Vugmeyster L, McKnight CJ (2009) Phosphorylation-induced changes in backbone dynamics of the dematin headpiece C-terminal domain. J Biomol NMR 43:39–50 [PubMed: 19030997]

Vugmeyster L, Ostrovsky D (2011) Temperature dependence of fast carbonyl backbone dynamics in chicken villin headpiece subdomain. J Biomol NMR 50:119–127 [PubMed: 21416162]

Vugmeyster L, Ostrovsky D, Li Y (2010) Comparison of fast backbone dynamics at amide nitrogen and carbonyl sites in dematin headpiece C-terminal domain and its S74E mutant. J Biomol NMR 47:155–162 [PubMed: 20396930]

Vugmeyster L, Perazzolo C, Wist J, Frueh D, Bodenhausen G (2004) Evidence of slow motions by crosscorrelated chemical shift modulation in deuterated and protonated proteins. J Biomol NMR 28:173–177 [PubMed: 14755161]

Wang C, Palmer AG, 3rd (2002) Differential multiple quantum relaxation caused by chemical exchange outside the fast exchange limit. J Biomol NMR 24:263–268 [PubMed: 12522313]

Wang TZ, Cai S, Zuiderweg ERP (2003) Temperature dependence of anisotropic protein backbone dynamics. J Am Chem Soc 125:8639–8643 [PubMed: 12848571]

Wang TZ, Frederick KK, Igumenova TI, Wand AJ, Zuiderweg ERP (2005) Changes in calmodulin mainchain dynamics upon ligand binding revealed by cross-correlated NMR relaxation measurements. J Am Chem Soc 127:828–829 [PubMed: 15656608]

Wist J, Frueh D, Tolman JR, Bodenhausen G (2004) Triple quantum decoherence under multiple refocusing: slow correlated chemical shift modulations of C' and N nuclei in proteins. J Biomol NMR 28:263–272 [PubMed: 14752259]

Wist J, Perazzolo C, Bodenhausen G (2005) Slow motions in nondeuterated proteins: Concerted chemical shift modulations of backbone nuclei. Appl Magn Reson 29:251

Yang DW, Mittermaier A, Mok YK, Kay LE (1998) A study of protein side-chain dynamics from new H2 auto-correlation and C-13 cross-correlation NMR experiments: Application to the N-terminal SH3 domain from DRK. J Mol Biol 276:939–954 [PubMed: 9566198]

Yao L, Vogeli B, Torchia DA, Bax A (2008a) Simultaneous NMR study of protein structure and dynamics using conservative mutagenesis. J Phys Chem B 112:6045–6056 [PubMed: 18358021]

Yao L, Vogeli B, Ying J, Bax A (2008b) NMR determination of amide N-H equilibrium bond length from concerted dipolar coupling measurements. J Am Chem Soc 130:16518–16520 [PubMed: 19049453]

Yao LS, Grishaev A, Cornilescu G, Bax A (2010) Site-specific backbone amide N-15 chemical shift anisotropy tensors in a small protein from liquid crystal and cross-correlated relaxation measurements. J Am Chem Soc 132:4295–4309 [PubMed: 20199098]

Ye CH, Fu RQ, Hu JZ, Hou L, Ding SW (1993) C-13 Chemical-shift anisotropies of solid amino-acids. Magn Reson Chem 31:699–704

Yee AW et al. (2016) Impact of deuteration on the assembly kinetics of transthyretin monitored by native mass spectrometry and implications for amyloidoses. Angew Chem Int Ed 55:9292–9296

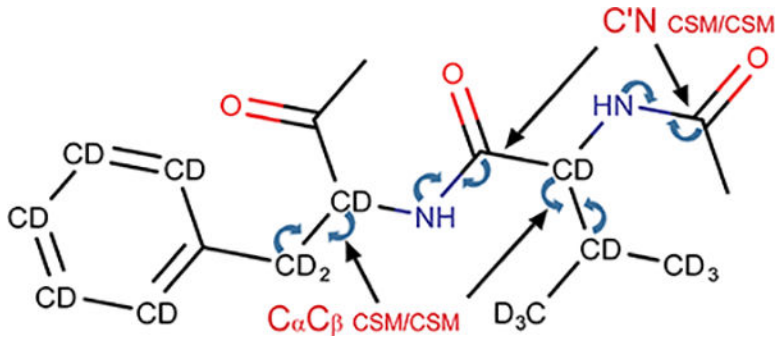

Figure 1.

Schematic representation of a dipeptide chain (ValPhe) depicting the deuteration pattern as well as the location of sites probed in the $^{13}C'$—^{15}N and $^{13}C_{\alpha}$—$^{13}C_{\beta}$ cross-correlated chemical shift modulation experiments.

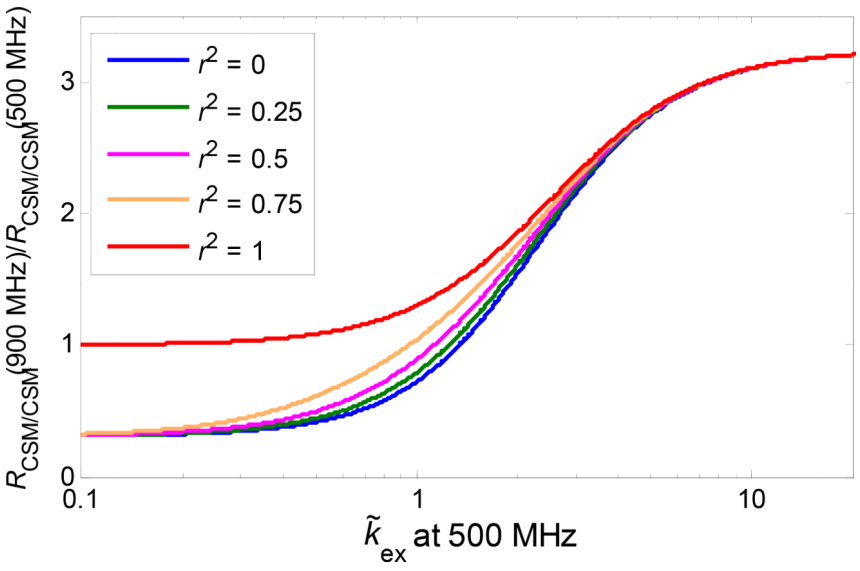

Figure 2.

Ratio of $R_{CSM/CSM}$ contributions calculated according to Eq. 6 at 900 and 500 MHz magnetic field strength versus, $\tilde{k}_{ex} = \frac{k_{ex}}{\sqrt{\Delta\omega_A^2 + \Delta\omega_B^2}}$ taken at 500 MHz for several values of the parameter $r = \frac{2\Delta\omega_A\Delta\omega_B}{\Delta\omega_A^2 + \Delta\omega_B^2}$. The line for $r^2 = 0$ is shown as the limiting case.

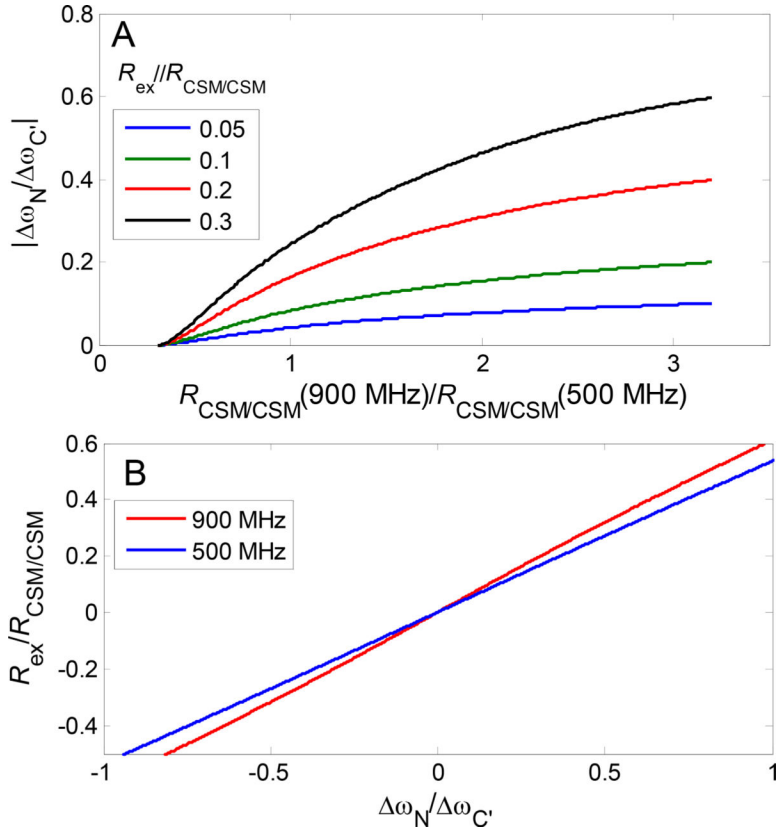

Figure 3.

A) Limits of $|\Delta\omega_N/\Delta\omega_{C'}|$ necessary to maintain the $R_{ex}/R_{CSM/CSM}$ ratio for different threshold levels shown on the graph as a function of $R_{CSM/CSM}$ at 900/$R_{CSM/CSM}$ at 500 calculated for ^{13}C'–^{15}N MQ and ^{15}N SQ R_{ex} measurements according to Eqs. 6,7. B) $R_{ex}/R_{CSM/CSM}$ ratio as a function of $\Delta\omega_N/\Delta\omega_{C'}$ for 500 (blue line) and 900 MHz (red line) field strengths with $R_{CSM/CSM}$ at 900/ $R_{CSM/CSM}$ at 500 =2.7, which corresponds to the weighted average over all residues in protonated GB3 at 25 °C.

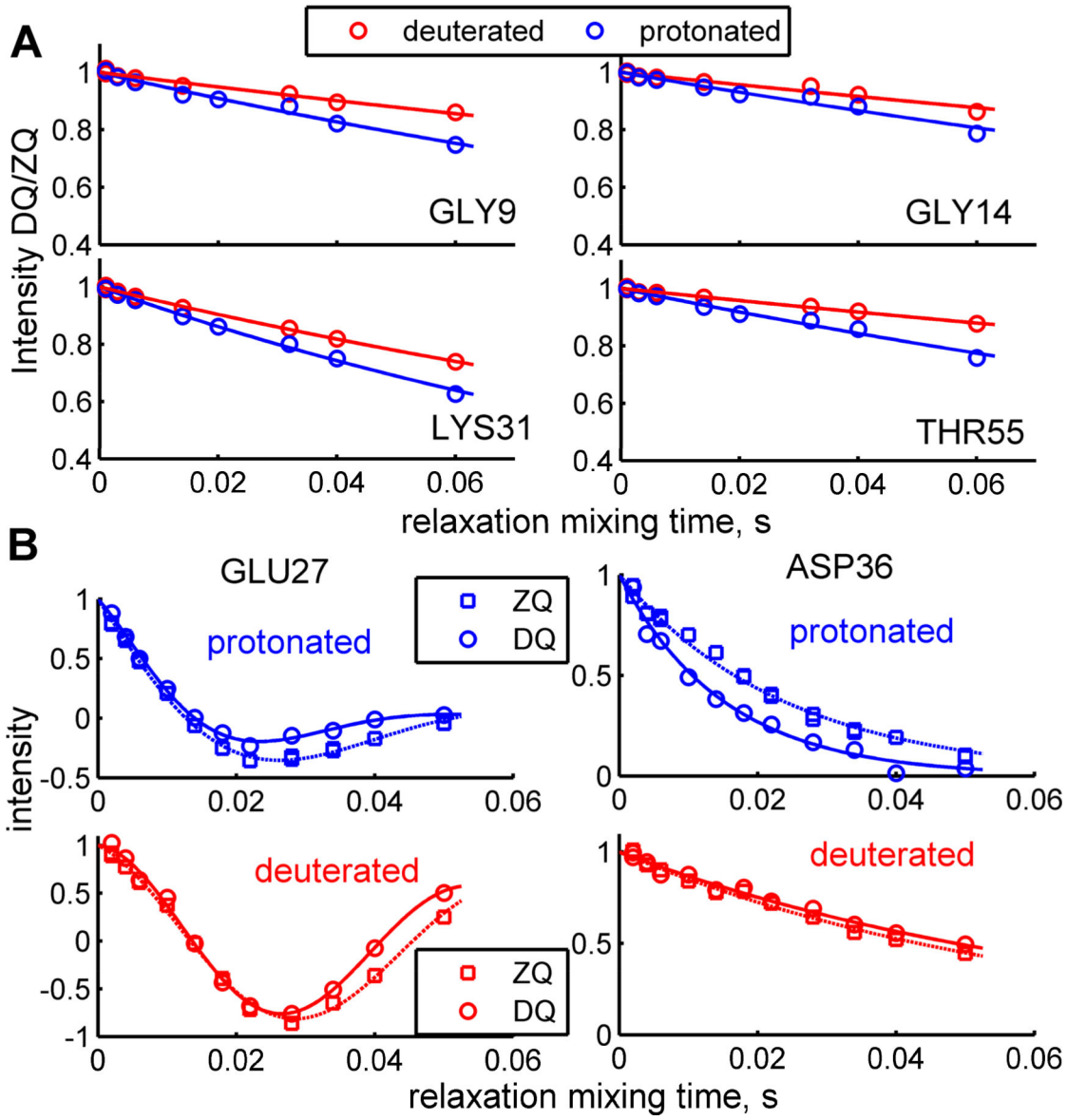

Figure 4.

A) C'N experiment. Ratio of intensities obtained from the ZQ and DQ spectra as a function of relaxation delay mixing time, **τ**. Solid lines represent fits to a mono-exponential function. B) CACB experiment. Intensities corresponding to DQ (circles) and ZQ (squares) as a function of relaxation delay mixing time, **τ** for protonated and deuterated GB3. The lines represent mono-exponential fits to the data for ASP36 (no aliphatic C_γ) or mono-exponential fits modulated by ($\cos\pi J_{eff}\,\tau$) to account for active coupling to the aliphatic C_γ carbon for GLU27; solid lines represent DQ data fits, and dotted lines ZQ. Data shown were collected at 25 °C and 500 MHz.

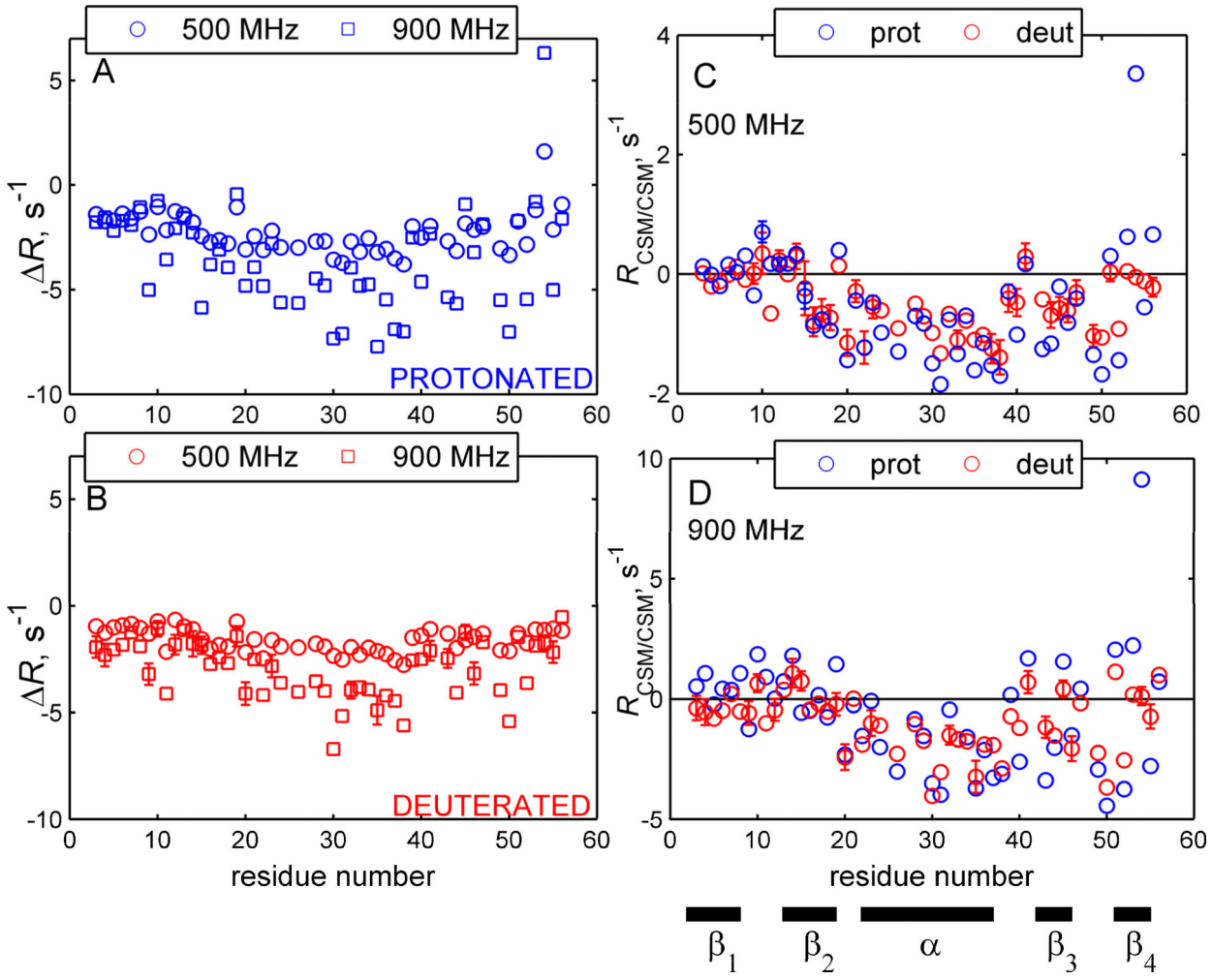

Figure 5.

Experimental differential cross-correlated relaxation rates ΔR for backbone $^{13}C'—^{15}N$ pairs in GB3 at 25 °C versus residue number. ΔR for the protonated (A) and deuterated (B) proteins at 500 (circles) and 900 MHz (squares). $R_{CSM/CSM}$ at 500 (C) and 900 MHz (D) for the protonated (blue circles) and deuterated (red circles) proteins. The numbering of residues corresponds to the amide nitrogen. Secondary structure elements are marked with rectangles below panel D. Error bars in $R_{CSM/CSM}$ plots are taken from experimental uncertainties in ΔR only and are not shown for values smaller than the size of the symbols.

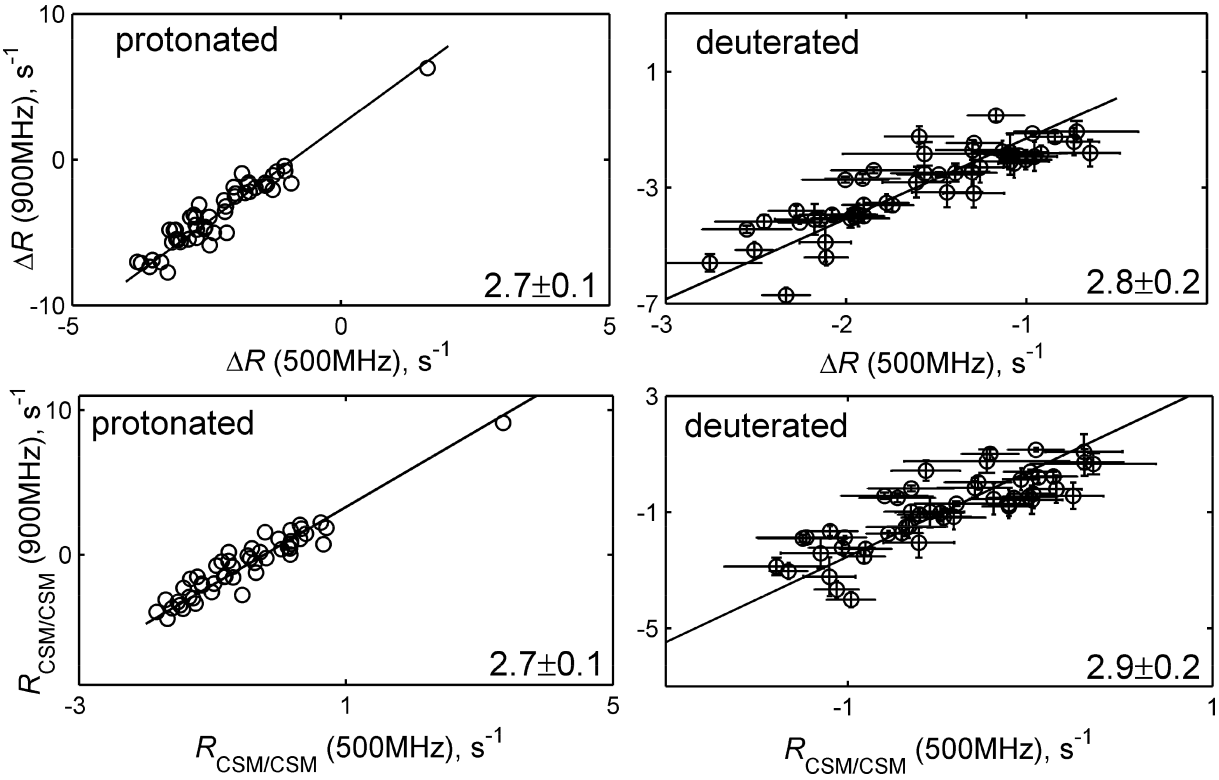

Figure 6.

Correlation plots of the $^{13}C'—^{15}N$ relaxation rates in GB3 at 25 °C at 900 and 500 MHz fields strengths. ΔR (top panels) and $R_{CSM/CSM}$ (bottom panels) for the protonated and deuterated proteins. Lines represent weighted linear regressions with the slope values shown in the lower right corner of each panel. Error bars for the protonated protein data are smaller than the sizes of the symbols and are not shown.

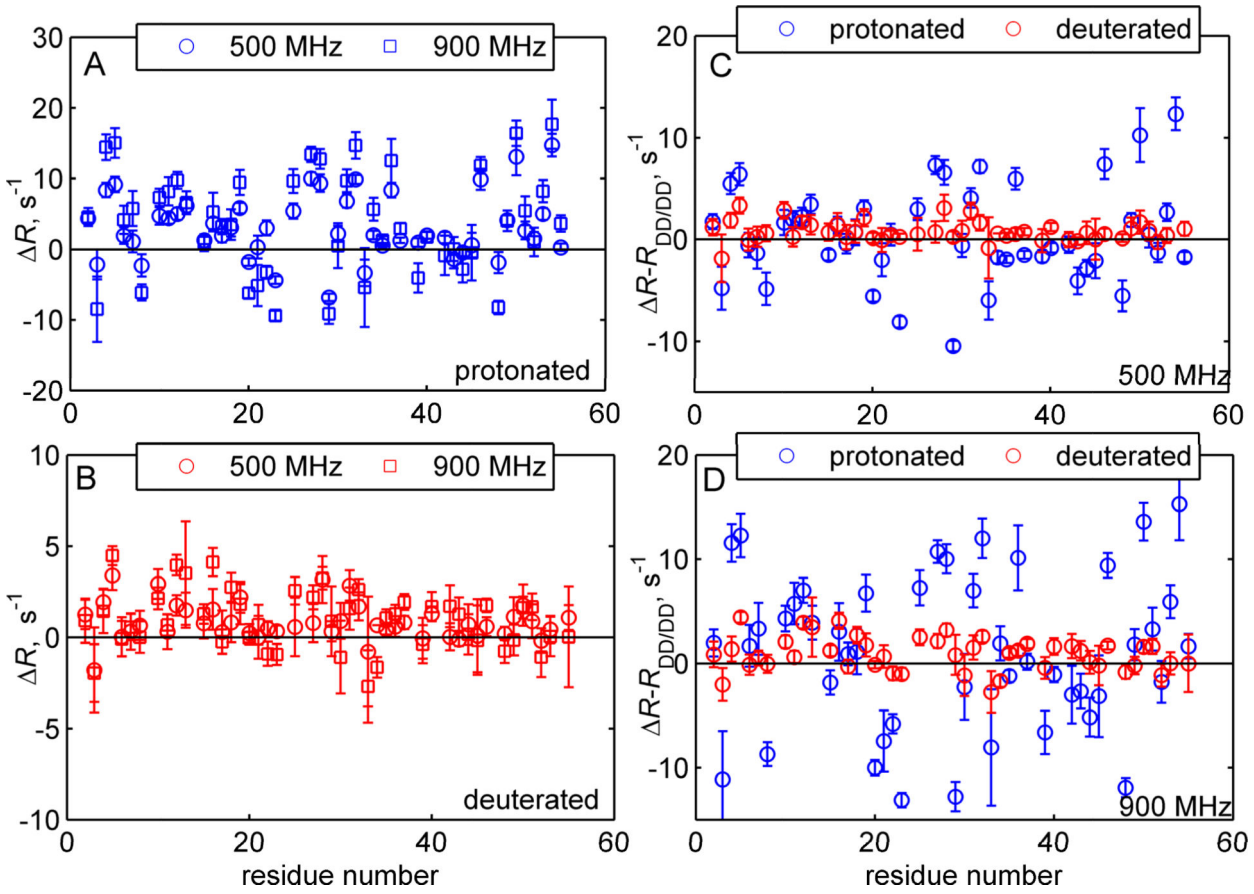

Figure 7.

Experimental rates from the $^{13}C_{\alpha}$—$^{13}C_{\beta}$ cross-correlated relaxation measurements in GB3 at 25 °C versus residue number. ΔR are shown for the protonated (A) and deuterated (B) proteins at 500 (circles) and 900 (squares), and ΔR —$R_{DD/DD}$ at 500 MHz (C) and 900 MHz (D) for the protonated (blue circles) and deuterated (red circles) proteins. The numbering of residues corresponds to C_{α} atoms. Error bars in $R_{CSM/CSM}$ plots are taken from experimental uncertainties in ΔR only.

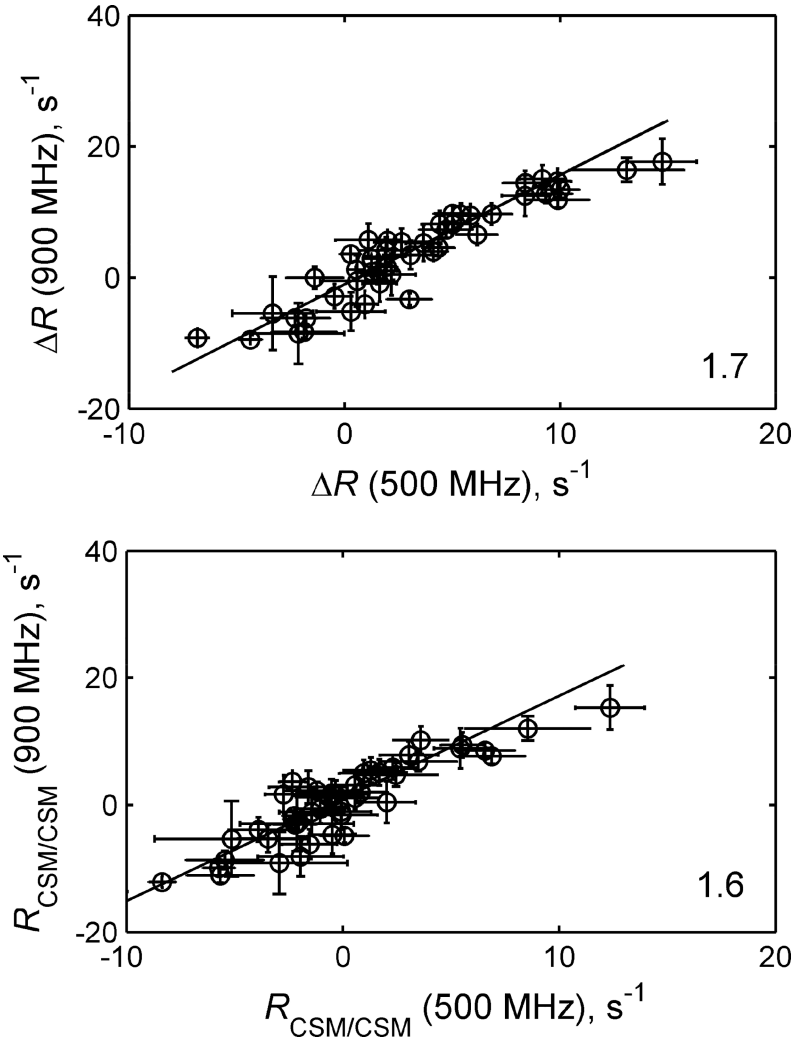

Figure 8.

Correlation plots for $^{13}C_{\alpha}$—$^{13}C_{\beta}$ rates in protonated GB3 at 25 °C at 900 and 500 MHz fields strengths. ΔR (top panel) and $R_{CSM/CSM}$ calculated according to Eq. 12 (bottom panel). Lines represent weighted linear regression with the slope values shown in the lower right corner of each panel.

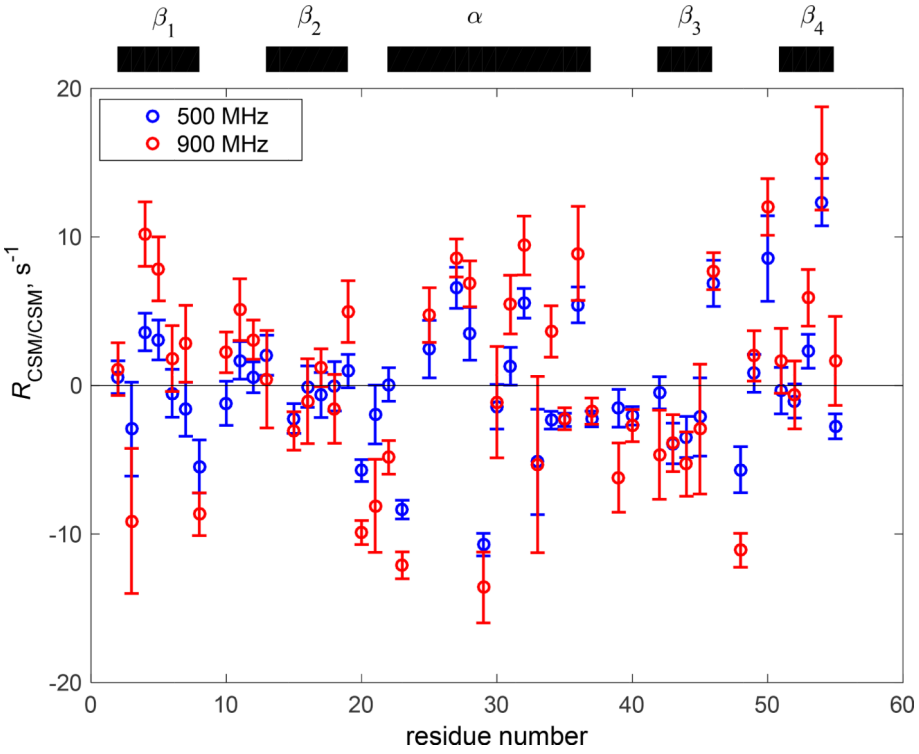

Figure 9.

$^{13}C_\alpha$—$^{13}C_\beta$ $R_{CSM/CSM}$ rates versus residue number in protonated GB3 protein at 25°C at 900 (red) and 500 (blue) MHz fields strengths, calculated according to Eq. 14. The numbering of residues corresponds to C_α atoms. Secondary structure elements are marked with rectangles.

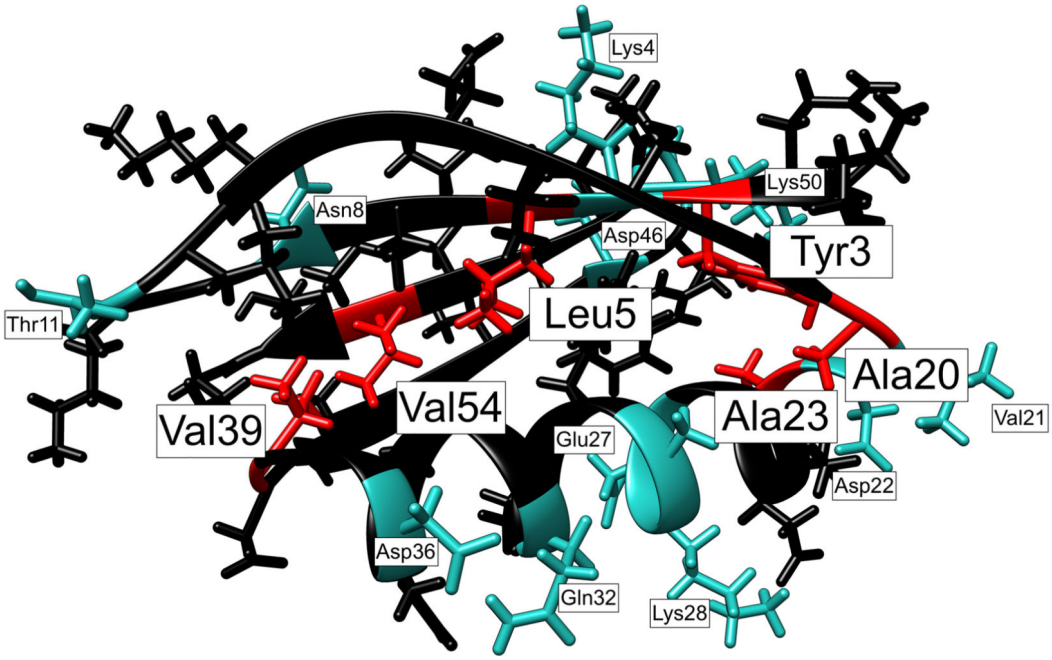

Figure 10.

Ribbon diagram of GB3 highlighting side-chains with relatively high $^{13}C_{\alpha}$—$^{13}C_{\beta}$ $R_{CSM/CSM}$ rates ($\gtrsim s^{-1}$ at 900 MHz) in the protonated sample: solvent-exposed (blue) and buried hydrophobic (red).

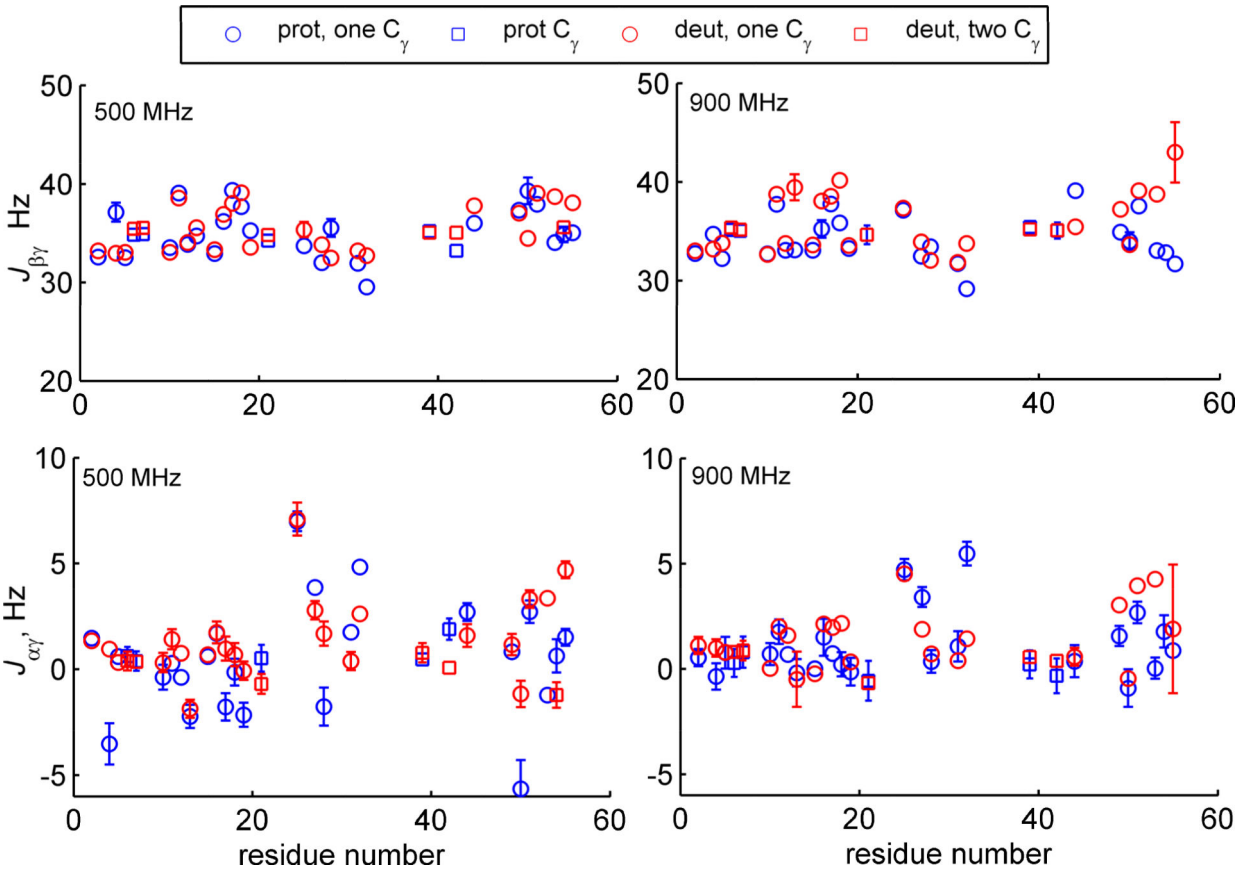

Figure 11.

Scalar coupling constants $^1J(C_\beta C_\gamma)$ (top panels) and $^2J(CaC_\gamma)$ (bottom panels) for side-chains with aliphatic C_γ carbons versus residue number, for GB3 at 500 and 900 MHz field strengths and at 25 °C. Error bars smaller than the size of the symbols are not shown.

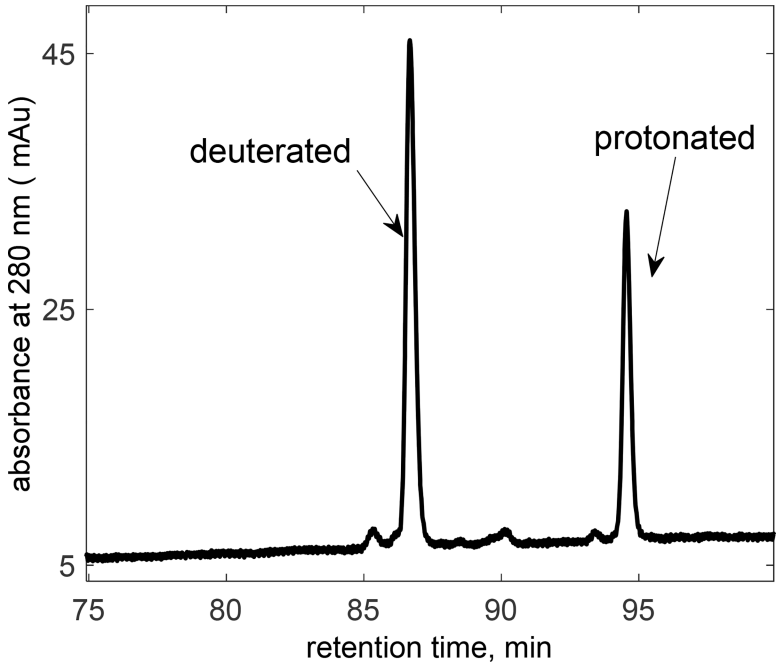

Figure 12.

Analytical RP-HPLC trace of a mixture of protonated and deuterated protein demonstrating the differences in the retention times. The profile was recorded on a C8 analytical column with 0.25% / min linear water/acetonitrile gradient with 0.05% TFA at 25 °C.